Chibby promotes ciliary vesicle formation and basal body docking during airway cell differentiation

Michael C. Burke,[1,2] Feng-Qian Li,[3,4] Benjamin Cyge,[3] Takeshi Arashiro,[5] Heather M. Brechbuhl,[6] Xingwang Chen,[3] Saul S. Siller,[2,3] Matthew A. Weiss,[7] Christopher B. O'Connell,[8] Damon Love,[3] Christopher J. Westlake,[7] Susan D. Reynolds,[6] Ryoko Kuriyama,[5] and Ken-Ichi Takemaru[1,2,3,4]

[1]Graduate Program in Genetics, [2]Medical Scientist Training Program, [3]Graduate Program in Molecular and Cellular Pharmacology, and [4]Department of Pharmacological Sciences, Stony Brook University, Stony Brook, NY 11794
[5]Department of Genetics, Cell Biology, and Development, University of Minnesota, Minneapolis, MN 55455
[6]Division of Cell Biology, Department of Pediatrics, National Jewish Heath, Denver, CO 80206
[7]Laboratory of Cell and Developmental Signaling, National Cancer Institute, Frederick, MD 21072
[8]Nikon Instruments, Inc., Melville, NY 11747

Airway multiciliated epithelial cells play crucial roles in the mucosal defense system, but their differentiation process remains poorly understood. Mice lacking the basal body component Chibby (Cby) exhibit impaired mucociliary transport caused by defective ciliogenesis, resulting in chronic airway infection. In this paper, using primary cultures of mouse tracheal epithelial cells, we show that Cby facilitates basal body docking to the apical cell membrane through proper formation of ciliary vesicles at the distal appendage during the early stages of ciliogenesis. Cby is recruited to the distal appendages of centrioles via physical interaction with the distal appendage protein CEP164. Cby then associates with the membrane trafficking machinery component Rabin8, a guanine nucleotide exchange factor for the small guanosine triphosphatase Rab8, to promote recruitment of Rab8 and efficient assembly of ciliary vesicles. Thus, our study identifies Cby as a key regulator of ciliary vesicle formation and basal body docking during the differentiation of airway ciliated cells.

Introduction

Cilia (primary or multicilia) are evolutionarily conserved microtubule-based organelles that protrude from the apical cell surface to perform diverse biological functions (Nigg and Raff, 2009; Goetz and Anderson, 2010; Hildebrandt et al., 2011). They are classified according to their microtubule composition, with the 9+0 microtubule arrangement in primary cilia and the 9+2 architecture in multicilia. Primary cilia are present on a wide range of cell types and play crucial roles in mechanosensation, photoreception, and intracellular signaling. Multicilia are mainly found on epithelial cells lining airways, reproductive tracts, and ependyma. They are important for clearing mucus and debris from the airway, transporting eggs from ovary to uterus, and circulating cerebrospinal fluid in the brain. Although the mode of centriole generation differs, formation of both types of cilia is thought to follow largely parallel pathways (Dawe et al., 2007; Vladar and Stearns, 2007). Genetic defects in the structure and function of cilia are associated with numerous human diseases including polycystic kidney disease, Bardet–Biedl syndrome, and primary ciliary dyskinesia, collectively known as ciliopathies (Nigg and Raff, 2009; Goetz and Anderson, 2010; Hildebrandt et al., 2011). Thus, deeper insights into the cellular and molecular mechanisms that control ciliogenesis have important implications for understanding the etiology of ciliopathies.

Within the centrosome of cycling cells, centrioles exist in pairs with one older mother and one immature daughter, which duplicate once per cell cycle using the existing centrioles as a template (canonical centriolar pathway; Nigg and Raff, 2009). The mother centriole is distinguished from the daughter centriole by the presence of subdistal and distal appendages. A single primary cilium is nucleated from the distal end of the mother

Correspondence to Ken-Ichi Takemaru: ken-ichi.takemaru@stonybrook.edu

Abbreviations used in this paper: ALI, air–liquid interface; Cby, Chibby; CCD, charge-coupled device; CCSP, Clara cell secretary protein; co-IP, coimmunoprecipitation; GEF, guanine nucleotide exchange factor; HPA, *Helix pomatia* agglutinin; IFT, intraflagellar transport; KO, knockout; MTEC, mouse tracheal epithelial cell; SEM, scanning EM; SIM, structured illumination microscopy; STORM, stochastic optical reconstruction microscopy; WT, wild type.

The Rockefeller University Press $30.00
J. Cell Biol. Vol. 207 No. 1 123–137
www.jcb.org/cgi/doi/10.1083/jcb.201406140

centriole during interphase of the cell cycle. On the other hand, multiciliated cells have the unique property of producing hundreds of centrioles through both centriolar and acentriolar pathways. It is thought that the majority of centrioles arise acentriolarly from deuterosomes, fibrogranular structures of unknown origin, whereas some are generated via the centriolar pathway (Sorokin, 1968; Dirksen, 1991; Klos Dehring et al., 2013). For simplicity, we will use the term centriole to refer to the organelle in the cytoplasm and basal body to refer to the organelle at the base of cilia. The centrioles mature by acquiring accessory structures, including subdistal and distal appendages (or transition fibers at the ciliary base), migrate, and dock to the apical cell surface. The distal appendages are thought to be critical for linking basal bodies to the plasma membrane (Czarnecki and Shah, 2012; Reiter et al., 2012). Nine distal appendage fibers emanate outwards and upwards from each of the B tubules of the centriole triplet microtubules, forming a pinwheel-like structure. In all types of cilia, the extension of cilium from each basal body, and its subsequent maintenance, require intraflagellar transport (IFT), a bidirectional transport system that tracks along the axonemal microtubules (Rosenbaum and Witman, 2002).

The molecular mechanisms of basal body docking remain poorly defined. A detailed EM study on differentiating ciliated cells in rat embryonic lungs suggests that before basal body docking, small vesicles most likely derived from the Golgi apparatus are recruited and attach to the distal appendages of centrioles (Sorokin, 1968). Subsequently, they fuse with each other to form a large membranous cap, the so-called ciliary vesicle, at the distal end of centrioles. Recently, using RPE1 cultured cells that form primary cilia upon serum starvation, it was demonstrated that the distal appendage protein CEP164 is indispensable for the docking of vesicles at the distal appendages (Schmidt et al., 2012). CEP164 forms a complex with the vesicular trafficking machinery components, the small GTPase Rab8 and its guanine nucleotide exchange factor (GEF) Rabin8. As centrioles migrate toward the cell surface, the ciliary vesicle undergoes fusion with apical membranes, allowing the centrioles to anchor to the cell surface. However, the molecular components, assembly, and exact function of ciliary vesicles in basal body docking remain obscure. As an alternative or parallel route, the direct attachment of distal appendages to cell membranes may take place without involvement of a ciliary vesicle. For primary cilia, migration and docking of basal bodies to cell membranes typically occur in columnar epithelial cells (Sorokin, 1968), but in other cell types, such as fibroblasts and smooth muscle cells, basal bodies lie at the cell center near the nucleus while extending cilia (Sorokin, 1962).

Chibby (Cby) is a 15-kD coiled-coil protein that is conserved in all ciliated unikont animals (except for nematodes) and their closest unicellular relative, the choanoflagellate *Monosiga brevicollis*, but is missing in most bikonts (Takemaru et al., 2003; Enjolras et al., 2012). We demonstrated that Cby knockout (KO) mice suffer from chronic respiratory infection as a result of a lack of mucociliary clearance, resulting from a marked reduction in the number of airway multicilia (Voronina et al., 2009; Love et al., 2010). Consistent with this phenotype, the Cby protein is detected at the base of cilia, indicating that Cby plays a direct role in ciliogenesis. More recently, using mammalian cell culture models, we found that Cby localizes to the distal end of mother centrioles and basal bodies and is required for formation of primary cilia (Steere et al., 2012). In *Drosophila melanogaster*, Cby is exclusively expressed in sensory neurons and male germ cells, the only ciliated cell types, and is associated with the transition zone, a compartment at the base of cilia (Enjolras et al., 2012). Cby mutant flies show defective sensory transduction and male hypofertility, resulting from abnormal cilia formation and function. However, the precise molecular function of Cby during ciliogenesis remains largely unknown.

Here, we report that Cby is essential for efficient docking of basal bodies to the apical cell surface in airway ciliated cells. In mature CbyKO ciliated cells, many centrioles fail to anchor to the apical membrane and cluster in the cytoplasm. Cby associates with the distal appendages of migrating centrioles, and loss of Cby impairs assembly of ciliary vesicles at the distal end of centrioles. Moreover, we demonstrate that Cby interacts with CEP164 and Rabin8 to promote the timely recruitment of Rab8 vesicles to the centrioles before docking to the apical membrane. Collectively, our results suggest that Cby acts in ciliary vesicle formation via the Rabin8–Rab8 membrane trafficking pathway to ensure efficient basal body docking during airway ciliated cell differentiation.

Results

Cby localization during differentiation of ciliated cells

Using unbiased stereological approaches, we confirmed and extended our previous findings that there is a significant decrease (~60%) in airway cilia in CbyKO mice compared with wild-type (WT) mice (Fig. S1, A and B). After naphthalene injury, which causes loss of cilia (Mahvi et al., 1977), CbyKO mice consistently showed a reduction in airway cilia on recovery day 13. To further explore Cby function in airway ciliated cells, we turned to the tracheal system because ciliated cells are highly abundant and primary cell culture models are available. Initial histological examination of the tracheal epithelium from CbyKO mice at various ages showed a consistent reduction in cilia (unpublished data). In agreement with this, in CbyKO tracheal explants, the rate of cilia-driven transport was markedly reduced (Fig. S1 C), and the distal-proximal directionality was also perturbed (Fig. S1 D). These data corroborate our previous findings that ablation of Cby results in a paucity of cilia and defective mucociliary activity in airways.

To determine the localization of Cby protein more precisely and gain insights into its molecular function, we adapted the mouse tracheal epithelial cell (MTEC) culture system originally developed by You et al. (2002). In this system, isolated tracheal cells seeded at low density on semipermeable membranes proliferate into a confluent, polarized epithelium in the first 5–7 d. Subsequently, differentiation is induced upon creation of air–liquid interface (ALI) conditions, and differentiation of the ciliated cell lineage proceeds in a semisynchronized fashion. Within 9–14 d after ALI, MTEC cultures are composed

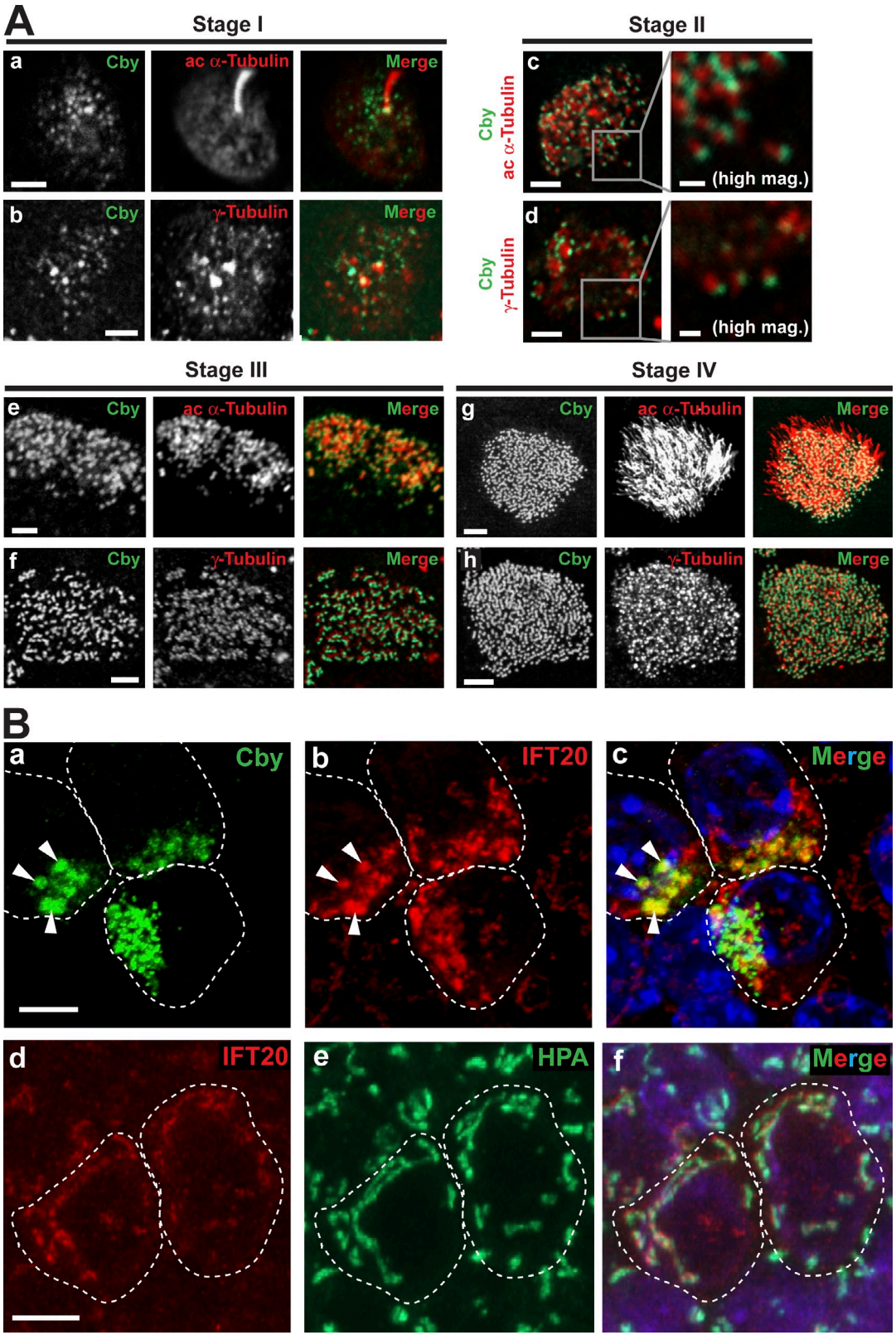

Figure 1. **Cby localization at different stages of ciliated cell differentiation.** (A) MTECs were colabeled at the indicated ciliogenesis stages with antibodies against Cby and the centriole/basal body/ciliary axoneme marker acetylated (ac) α-tubulin or the centriole/basal body marker γ-tubulin. Essentially, immunostaining of CbyKO MTECs with the Cby antibody produced no signals (not depicted) confirming the antibody specificity. Bars: (main images) 2 µm; (high magnification images for stage II) 0.5 µm. See also Fig. S2 A. (B) Stage II MTECs were costained with Cby and IFT20 antibodies (a–c) or with the IFT20 antibody and the cis-medial Golgi marker lectin HPA (d–f). Nuclei in the merged image were visualized by DAPI (blue). (a–c) Arrowheads indicate areas of diffuse Cby staining that prominently overlap with IFT20. (d–f) In ciliated cells, IFT20 also showed Golgi localization. Dashed lines demarcate cell boundaries. Bars, 5 µm. See also Fig. S2 B.

of ciliated cells (typically 30–50%) and nonciliated cells and resemble the native tracheal epithelium.

MTECs were fixed at different post-ALI days and costained with antibodies against Cby (Cby8-2; Cyge et al., 2011) and the centriole/basal body/ciliary axoneme marker acetylated α-tubulin or the centriole/basal body marker γ-tubulin (Fig. 1 A). Four different stages of centriole formation (stages I–IV) were identified based on the criteria described previously (Vladar and Stearns, 2007). Approximately 2 d after ALI creation (ALId2), stage I ciliated cell differentiation was noted, and elongated primary cilia were visible. At this stage, Cby appeared as numerous cytoplasmic foci, characteristic of typical centrosomal proteins (Fig. 1 A, a and b; Vladar and Stearns, 2007). Throughout stages II and III, as centrioles replicated en masse and migrated toward the apical plasma membrane, Cby was closely associated with centrioles (Fig. 1 A, c–f). High-magnification views at stage II revealed close apposition of Cby to acetylated α-tubulin– and γ-tubulin–positive centrioles. At stage IV during which axoneme growth occurred, an intense Cby signal was detected at the basal bodies and maintained in mature ciliated cells (Fig. 1 A, g and h). Furthermore, an intimate spatial relationship between Cby and centrin, which marks the distal lumen of centrioles/basal bodies, was observed in ciliated cells in MTEC cultures prepared from transgenic mice expressing GFP–centrin-2 (Fig. S2 A; Higginbotham et al., 2004).

During the course of our localization experiments, we occasionally noticed relatively large areas of diffuse Cby staining in ciliated cells at early differentiation stages (Fig. 1 B, a, arrowheads). To evaluate whether these Cby-positive acentriolar structures coincide with the Golgi complex, we colabeled Cby with the Golgi markers IFT20 (an IFT subunit, which resides mainly in the cis-medial Golgi compartment; Follit et al., 2006), GM130 (cis-Golgi), GMAP210 (cis-Golgi), and syntaxin 6 (trans-Golgi). The diffusely Cby-stained areas showed extensive colocalization with IFT20 (Fig. 1 B, a–c, arrowheads) but not with the other Golgi markers (Fig. S2 B). We speculate that these subcellular compartments may represent pools of post-Golgi vesicles potentially involved in the assembly of centrioles. Through costaining with the cis-medial Golgi marker *Helix pomatia* agglutinin (HPA), we observed the Golgi localization of IFT20 in differentiating ciliated cells (Fig. 1 B, d–f) as previously reported in IMCD3 and RPE1 cells (Follit et al., 2006), typically at more basal confocal planes than replicating centrioles. Cby localization in close association with centrosomal/ciliary proteins throughout differentiation implies a key role in regulating ciliogenesis in airway ciliated cells.

The C-terminal coiled-coil motif of Cby mediates basal body targeting

Cby is a small protein of 15 kD (126 aa in humans) with no significant homology to any known proteins (Fig. 2 A; Takemaru et al., 2003). The C-terminal half of Cby contains a conserved leucine zipper coiled-coil motif essential for its homodimerization (Mofunanya et al., 2009). Having established that Cby is located at the centrioles/basal bodies during ciliated cell differentiation, we sought to determine which domain of Cby is responsible for this targeting. To this end, we infected MTECs prepared from tracheas of CbyKO mice with lentiviruses expressing Flag-tagged human full-length Cby (FL), the C-terminal portion (C; aa 49–126), or a Cby mutant deficient in homodimerization (4A), which contains alanine substitutions for four leucine residues within the coiled-coil motif (Mofunanya et al., 2009). Immunostaining with the Flag or Cby antibody and the γ-tubulin antibody at ALId14 revealed proper localization of Cby-FL at the basal bodies (Fig. 2 B). Cby-C was correctly recruited to the basal bodies, implying that the coiled-coil motif facilitates its basal body targeting. In accordance with this notion, Cby-4A exhibited diffuse cytoplasmic localization and failed to localize to the basal bodies. Western blotting showed that Cby-FL and Cby-4A were stably expressed, but Cby-C was detected at lower levels (Fig. 2 C). We concluded that the coiled-coil homodimerization motif is responsible for targeting of Cby to the basal bodies.

Cby clusters as rings at transition fibers and in the proximal region of the transition zone of mature cilia

Centrioles and basal bodies are barrel-shaped structures that are ∼200–250 nm in diameter and 400–500 nm in length (Sillibourne et al., 2011; Lau et al., 2012; Sonnen et al., 2012). Their dimensions are close to the diffraction limit of conventional optical microscopy, which is at best 200 nm in the lateral and 600 nm in the axial resolution. To visualize Cby localization at the superresolution level, we used 3D structured illumination microscopy (SIM; 3D-SIM), which achieves twofold higher resolution in each dimension than confocal microscopy. 3D-SIM imaging of Cby and cilia in fully differentiated ciliated cells revealed that Cby protein concentrated in ring-shaped patterns at the base of each cilium (Fig. 3 A and Video 1). The ring-like localization of Cby at the ciliary base is reminiscent of that of the distal appendage/transition fiber component CEP164 (Graser et al., 2007; Sillibourne et al., 2011; Lau et al., 2012; Sonnen et al., 2012), which is mutated in nephronophthisis-related ciliopathies (Chaki et al., 2012). Thus, we examined the spatial relationship of Cby and CEP164 in MTECs at ALId14 using 3D-SIM. Adjacent localization of the two proteins was observed at the apical cell surface (Figs. 3 B and S3). Consistent with a previous 3D-SIM study (Sonnen et al., 2012), some distinct density masses of CEP164 staining were recognizable. Intriguingly, Cby rings were slightly smaller than CEP164 rings and were positioned more apically (Fig. S3).

To further investigate the precise Cby localization, we performed preembedding immuno-EM on ALId14 MTECs using the Cby8-2 antibody (Fig. 3 C). Through a series of thin cross sections along basal bodies and cilia, electron-dense dots of Cby staining were particularly abundant toward the distal part of the transition fibers where they attached to the apical membrane (Fig. 3 C, h and i). Distal to the basal body is the transition zone, which is characterized by the presence of distinctive Y-shaped links that connect the doublet microtubules to the surrounding ciliary membrane and proposed to serve as a ciliary gate (Czarnecki and Shah, 2012; Reiter et al., 2012). Although Cby was rarely detectable in the distal region of the transition zone (Fig. 3 C, b and c), numerous intense Cby dots were

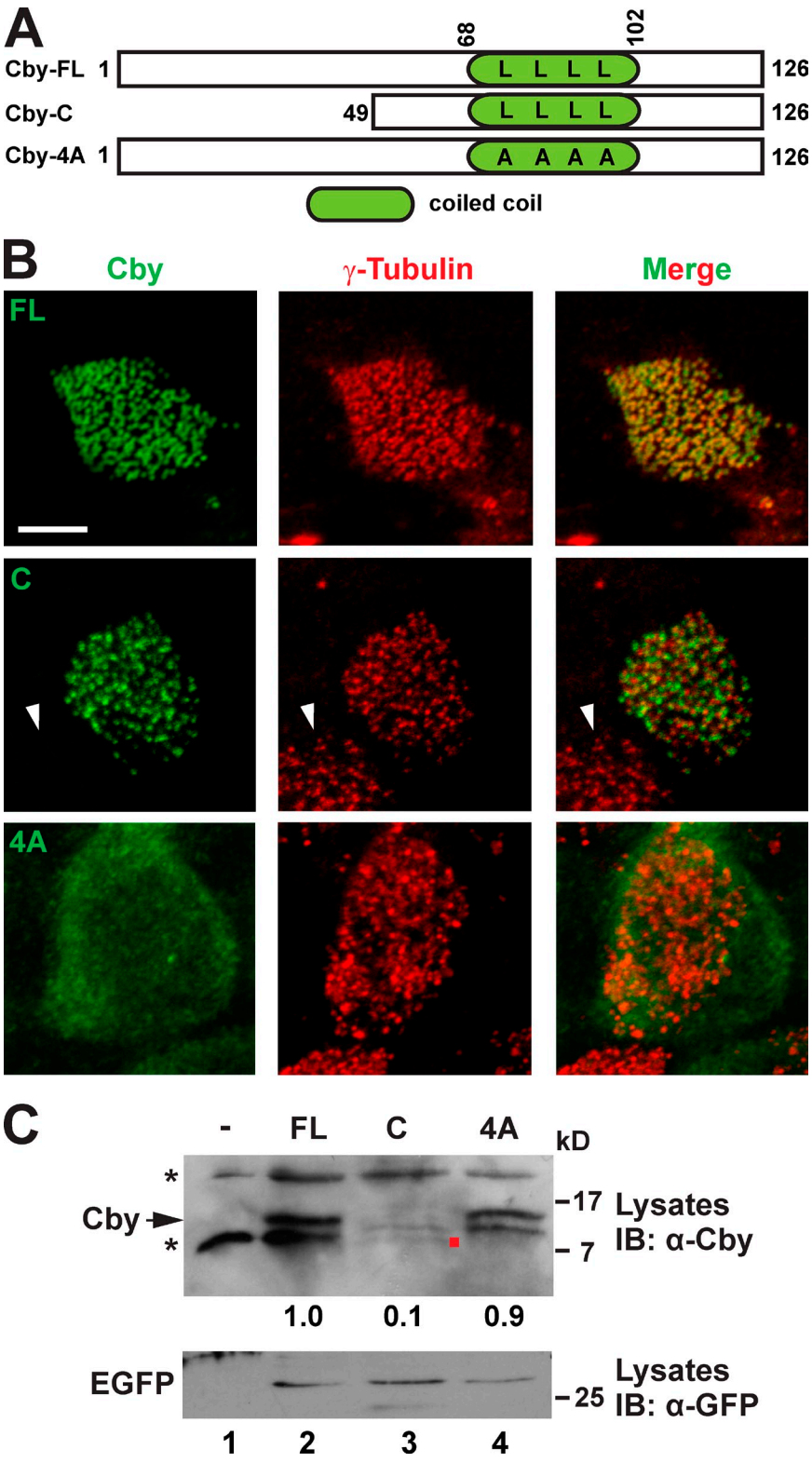

Figure 2. **The C-terminal coiled-coil motif is essential for Cby basal body localization.** (A) Schematic depiction of human Cby constructs used in this study. The numbers indicate amino acid positions. Four leucines at positions 77, 84, 91, and 98 crucial for Cby homodimerization are shown. The dimerization-defective Cby-4A mutant contains alanine substitutions for all four leucine residues. (B) CbyKO MTECs were infected with lentiviruses encoding human full-length Cby (FL), Cby-C containing a leucine zipper coiled-coil motif, or Cby-4A mutant and colabeled with Cby and γ-tubulin antibodies at ALId14. Note that no Cby fluorescence was seen in noninfected ciliated cells (arrowheads). Bar, 5 µm. (C) Western blotting for expression of Cby mutants. Cell lysates were prepared from uninfected or infected CbyKO MTECs at ALId14 and probed with the Cby antibody. Note that Cby-C was detected at low levels (red dot). The asterisks indicate nonspecific bands present in uninfected cell lysates. The lentiviral constructs expressed EGFP from internal ribosome entry site, and similar transduction rates were verified by Western blotting with the GFP antibody. The band intensity of Cby proteins was quantified and normalized to that of EGFP. The normalized value for FL-Cby was set as 1. IB, immunoblot.

present in the proximal segment (Fig. 3 C, e and f). Interestingly, Cby appeared to be preferentially enriched outside the doublet microtubules near the ciliary membrane. Besides these confined areas, we did not observe major sites of Cby clustering in mature ciliated cells. There were no signals detected in CbyKO-negative controls that were processed in parallel (Fig. 3 C, d, g, and j).

Because immuno-EM analysis is mostly limited to providing 2D information on thin sections, we used 3D stochastic optical reconstruction microscopy (STORM; 3D-STORM), which yields ≤20-nm lateral and ≤50-nm axial resolutions. Imaging of endogenous Cby at the base of cilia through 3D-STORM revealed that Cby molecules typically gathered into several discrete domains in a ring-shaped pattern (Fig. 3 D,

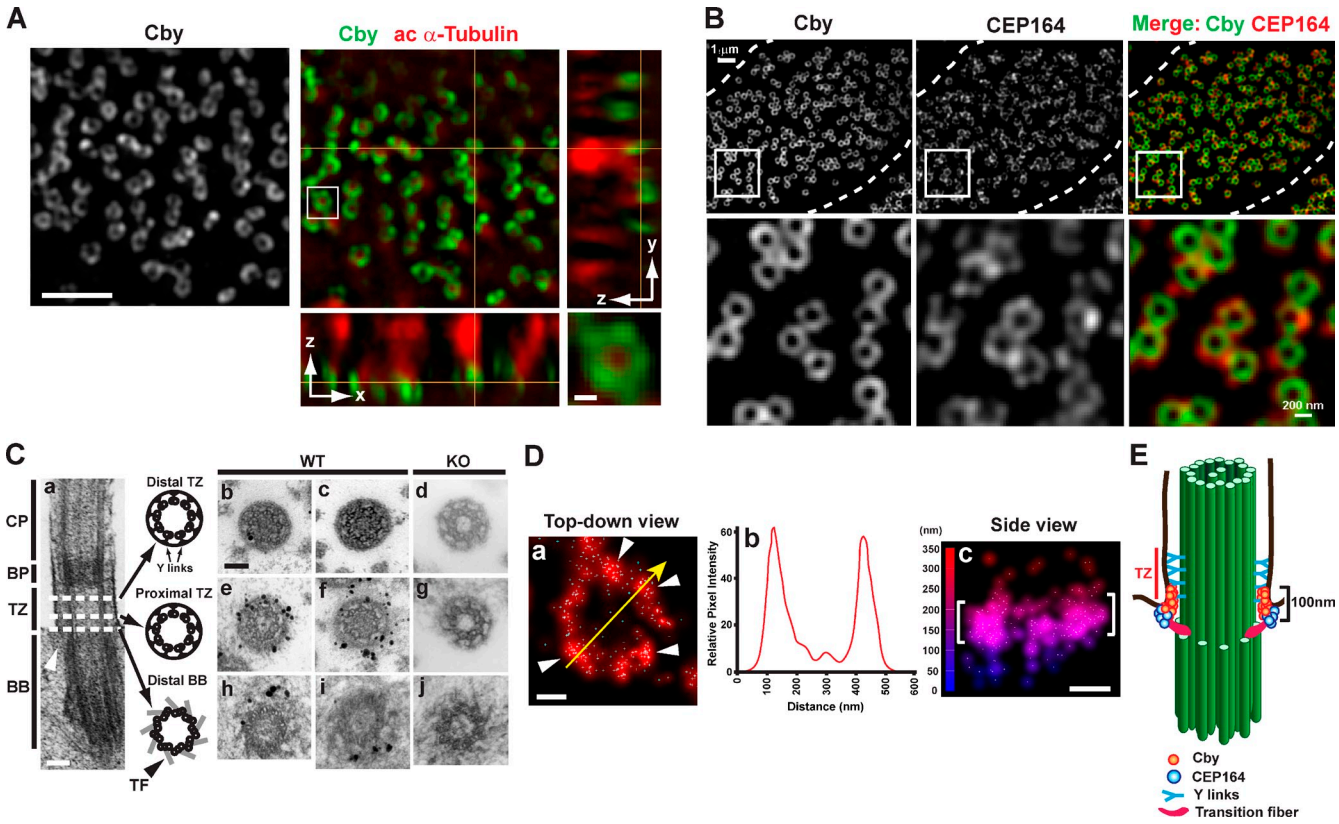

Figure 3. **Cby protein is enriched at transition fibers and in the proximal compartment of the transition zone of mature cilia.** (A) Fully differentiated MTECs at ALId14 were colabeled with antibodies for Cby and the ciliary axoneme marker acetylated (ac) α-tubulin and imaged by superresolution 3D-SIM. Top-down (x-y; single sections) and side (y-z on the right and x-z on the bottom; maximum projections) views are shown. The squared area is shown in higher magnification at the bottom right corner. See also Video 1. (B) Cby clusters as rings smaller than CEP164 rings at the ciliary base. Fully differentiated MTECs were costained with antibodies against Cby and CEP164 and imaged by 3D-SIM. The images are maximum projections from 10 z sections taken at 125-nm intervals. Top-down views and high-magnification views of the square areas are shown. Dashed lines demarcate cell boundaries. See also Fig. S3. (C) Immuno-EM localization of Cby in thin cross sections (80 nm) through the distal (b and c) and proximal (e and f) regions of the transition zone and the distal part of basal bodies (h and i) at the base of cilia in WT MTEC cultures at ALId14. (d, g, and j) CbyKO MTECs were processed in parallel as a negative control. A representative EM image of a cilium in longitudinal section is shown in a. Arrowheads in a denote the transition fiber. CP, cilia proper; BP, basal plate; TZ, transition zone; BB, basal body; TF, transition fiber. (D) Superresolution 3D-STORM images of Cby ring substructure in ALId14 MTEC cultures. Shown are a top-down view (a), intensity profile along the yellow arrow in a (b), and side view with a height map (c). White arrowheads in a point to Cby clusters. Brackets in c indicate the areas in which Cby molecules were highly enriched. The data are from a single representative experiment out of three repeats. (E) Cartoon depicting Cby localization at the base of mature cilia. Bars: (A, main image) 1 μm; (A [bottom right], C, and D) 0.1 μm.

arrowheads). An intensity profile of a yellow arrow across the Cby ring (Fig. 3 D) suggested that Cby clusters spaced around a ring of ∼300 nm in diameter (Fig. 3 D, b). Furthermore, a side view of the Cby ring demonstrated that Cby molecules were highly concentrated in a narrow zone, ∼100 nm high (Fig. 3 D, c). Collectively, our imaging experiments establish that the Cby protein clusters as rings (300 nm in diameter and 100 nm in height) near the distal portion of the transition fibers as well as in the proximal region of the transition zone near the ciliary membrane (Fig. 3 E).

CEP164 physically interacts with and recruits Cby to the mother centriole

The close proximity of Cby and CEP164 proteins at the distal end of basal bodies (Figs. 3 B and S3) and mother centrioles in RPE1 cells (Steere et al., 2012) prompted us to examine whether they interact directly. Coimmunoprecipitation (co-IP) analyses demonstrated a specific interaction between Cby and CEP164 (Fig. 4 B). To determine the region of CEP164 responsible for Cby binding, we performed co-IP assays using CEP164 deletion mutants. Although neither CEP164-N (aa 1–558) nor CEP164-M (aa 559–1,100) bound to Cby, CEP164-C (aa 1,101–1,460) was coimmunoprecipitated with Cby (Fig. 4 C). Further deletion experiments of this region revealed that Cby binds to the C-terminal fragment spanning aa 1,201–1,460 (CEP164-CC). CEP164-CC interacted firmly with the C-terminal region of Cby (C; aa 64–126) but exhibited greatly reduced binding to Cby-4A (Fig. 4 D). The N-terminal half of Cby (N; aa 1–63) was undetectable upon expression in HEK293T cells (Fig. 4 D, right) and could not be tested for interaction with CEP164. The poor solubility of recombinant proteins precluded us from determining a direct interaction between Cby and CEP164.

In CbyKO ciliated cells, CEP164 was correctly targeted to the basal bodies (Fig. S5 B). Hence, we considered the possibility that CEP164 might recruit Cby to the distal appendages/transition fibers. To test this, we turned to cell culture models in which endogenous Cby and CEP164 are present at the centrioles throughout the cell cycle. HeLa cells stably expressing GFP–centrin-1 (Steere et al., 2012) were treated either with CEP164 siRNA or all reagents except for siRNA (mock) followed by

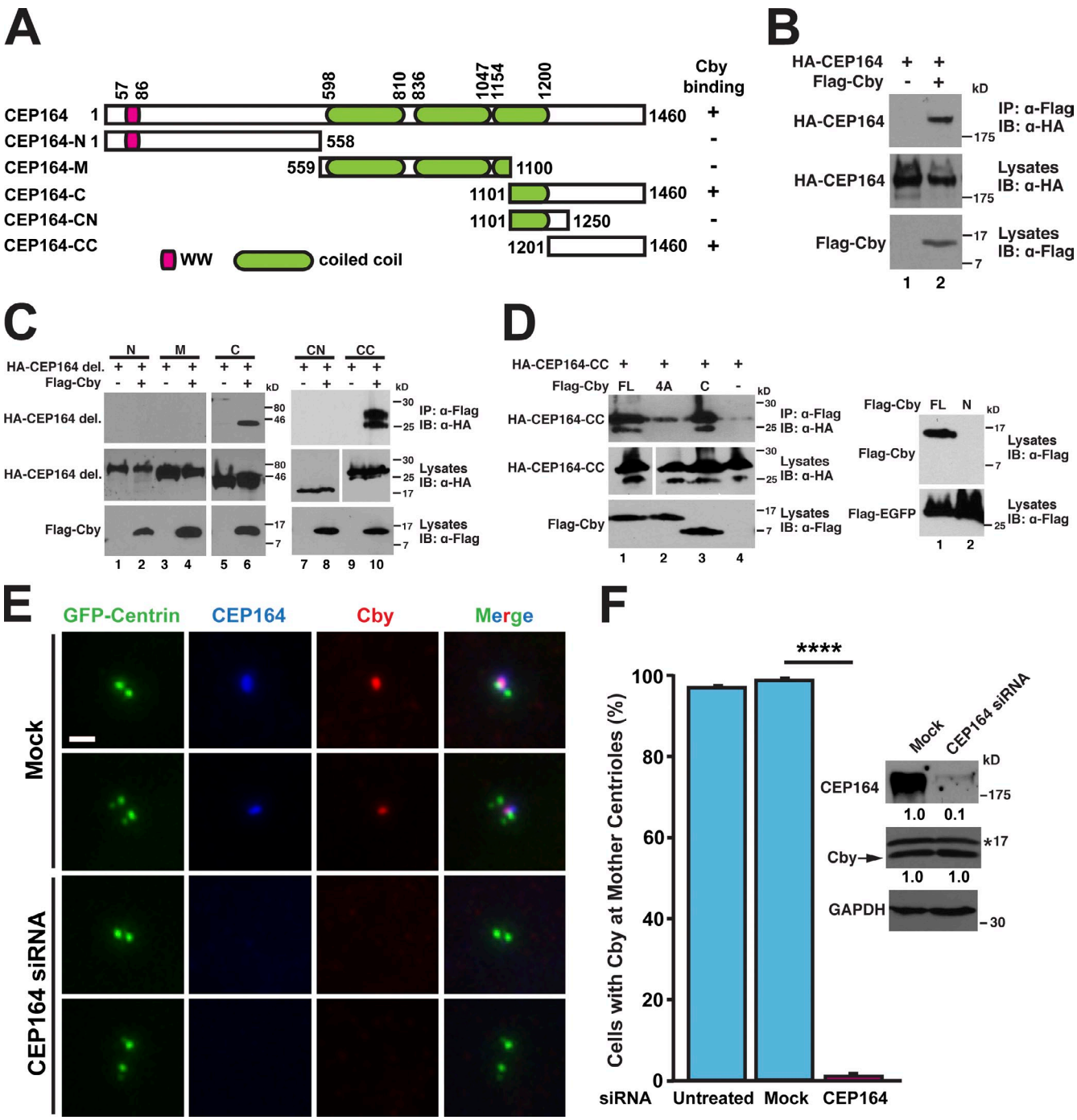

Figure 4. **CEP164 binds and recruits Cby to the distal appendages.** (A) Schematic diagram of CEP164 constructs used in this study. The numbers indicate amino acid positions. (B) HEK293T cells were transfected with HA-CEP164 and Flag-Cby expression constructs as indicated, and cell lysates were immunoprecipitated with the Flag antibody and immunoblotted with the HA antibody. Cell lysates were also probed with HA and Flag antibodies to show stable protein expression. (C) Cell lysates from HEK293T cells expressing Flag-Cby and the indicated HA-tagged CEP164 fragments were immunoprecipitated with the Flag antibody and detected with the HA antibody. del., deletion. (D) CEP164 binds to the C-terminal region of Cby. HEK293T cells were transfected with expression constructs for HA–CEP164-CC and Flag-tagged Cby-FL, -4A, or -C (aa 64–126), and cell lysates were immunoprecipitated with the Flag antibody and immunoblotted with the HA antibody. (right) The N-terminal half of Cby (aa 1–63) was undetectable upon transfection. Cells were co-transfected with an expression plasmid for Flag-EGFP to normalize for transfection efficiency. White lines indicate that intervening lanes have been spliced out. (E) HeLa cells expressing GFP–centrin-1 were mock treated (all reagents except for siRNA) or transfected with CEP164 siRNA and immunostained with CEP164 and Cby antibodies. Cells with a pair or two pairs of centrioles are shown for each siRNA. Bar, 1 µm. (F) Quantification of the number of cells with Cby at the mother centrioles after siRNA treatment. U2OS cells were untreated, mock transfected, or transfected with CEP164 siRNA for 27 h and immunostained for Cby and CEP164. A total of 811 (untreated), 595 (mock), and 856 (CEP164 siRNA) cells were counted from at least five independent experiments. Data are presented as means ± SD. ****, $P < 0.0001$. Expression levels of CEP164, Cby, and GAPDH were determined by Western blotting. The asterisk indicates nonspecific bands. The band intensities of CEP164 and Cby were quantified and normalized to those of GAPDH. The normalized values for mock-transfected samples were set as 1. IB, immunoblot; IP, immunoprecipitation.

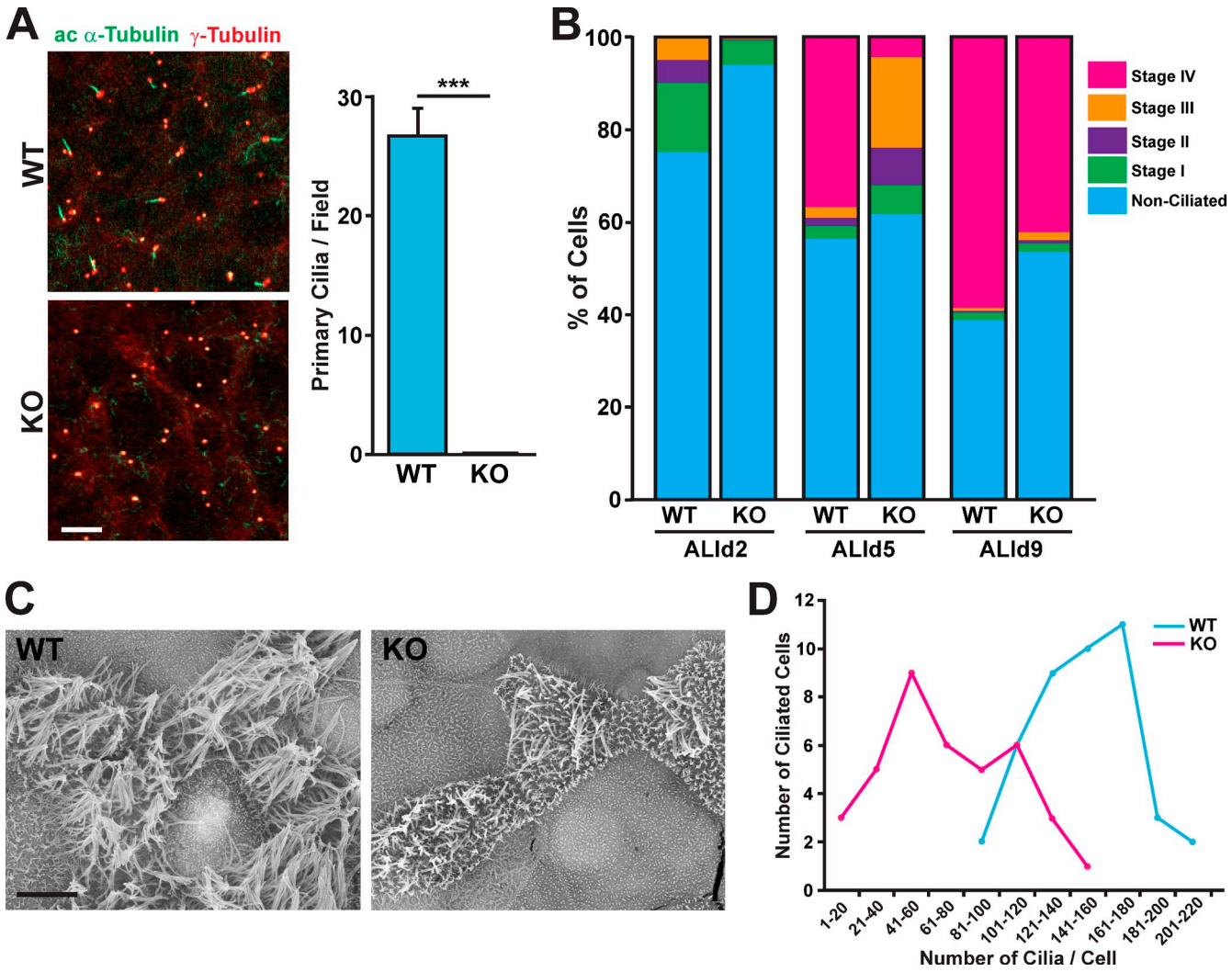

Figure 5. **Impaired ciliogenesis in CbyKO ciliated cells.** (A) WT and CbyKO MTECs were colabeled at ALId2 with acetylated (ac) α-tubulin and γ-tubulin antibodies. Bar, 10 µm. The quantification of primary cilia is shown in the graph on the right. For each genotype, primary cilia were counted in three microscopic fields (100× magnification) per MTEC preparation, and data are presented as means ± SEM from three independent MTEC preparations. ***, $P < 0.001$. (B) WT and CbyKO MTECs were fixed at ALId2, d5, and d9, and the percentage of cells in each stage of ciliogenesis were quantified based on immunostaining for acetylated α-tubulin and γ-tubulin. At least 600 cells/genotype/ALI day were counted from three independent MTEC preparations. See also Fig. S4. (C) Representative SEM images of WT and CbyKO ciliated cells in MTEC cultures at ALId9. Numerous short microvilli are apparent on the apical surface of CbyKO ciliated cells. Bar, 5 µm. (D) The number of cilia on ciliated cells was quantified on SEM images of MTEC cultures at ALId9, and the distribution of ciliated cells with numbers of cilia per cell was grouped into bins of 20. WT, $n = 43$; KO, $n = 39$.

immunostaining for Cby and CEP164 (Fig. 4 E). In mock-treated cells, Cby and CEP164 showed extensive colocalization at the mother centrioles. In contrast, CEP164 knockdown cells had no detectable centriolar Cby signals. To quantify the dependence of Cby centriolar localization on CEP164, we chose U2OS cells as a model system because siRNA-mediated gene silencing is effectively achieved. As shown in Fig. 4 F, 97.4% of untreated or 99.1% of mock-treated cells displayed normal Cby localization at the mother centrioles. In contrast, the vast majority of CEP164 siRNA-treated cells lost centriolar Cby, with only 1.1% having detectable levels of Cby at the centrioles. There was no major change in Cby protein levels upon CEP164 knockdown (Fig. 4 F). Similar results were obtained with ciliated RPE1 cells (Cby detected at basal bodies in only 0.82 ± 1.25% of CEP164-depleted cells compared with 97.87 ± 0.85% of mock-treated cells). These data indicate that the C-terminal region of CEP164 binds to the C-terminal coiled-coil domain of Cby and localizes it to the distal appendages.

CbyKO ciliated cells exhibit defective ciliogenesis

To better understand the role of Cby in the differentiation of airway ciliated cells, we prepared MTECs from tracheas of adult CbyKO mice and compared them with WT MTECs at different differentiation stages. Tracheal progenitor cells isolated from CbyKO mice grew normally on supported membranes and reached confluence at a rate similar to that of WT cells (unpublished data). At ALId0–2, in WT cultures, many primary cilia extending from basal bodies were noticeable as revealed by immunostaining for acetylated α-tubulin and γ-tubulin (27 primary cilia/field at ALId2; Fig. 5 A). Remarkably, no primary cilia were observed in CbyKO MTECs, although basal bodies were clearly detectable.

Next, we fixed CbyKO and WT MTECs at ALId2, d5, and d9 and immunostained with acetylated α-tubulin and γ-tubulin antibodies to determine the percentages of ciliating cells in each stage of ciliogenesis as previously described (Vladar and Stearns, 2007). As shown in Fig. 5 B, at ALId2, 25% of cells in WT MTEC cultures were at stages I–III, whereas only 8% of CbyKO cells had committed to the ciliated cell lineage, showing features of stage I with γ-tubulin foci near the centrosome in the apical cytoplasm. A similar trend was observed using an antibody for Foxj1, an early marker of ciliated cell differentiation (Fig. S4; Blatt et al., 1999). Ciliated cell differentiation in WT MTEC cultures proceeded robustly in the next 3 d. At ALId5, 37% of WT cells reached stage IV and started to extend cilia as indicated by the appearance of acetylated α-tubulin–positive axonemes. In contrast, only 4% of cells reached stage IV in CbyKO cultures at this time and 29% were still at stages I–III. At ALId9 when differentiation was almost completed, 58% of WT cells were at stage IV, whereas only 41% of CbyKO cells were at stage IV. A similar trend was maintained at ALId21 (unpublished data). We noticed that terminally differentiated ciliated cells in CbyKO cultures often exhibited variable, weak-to-moderate signal intensities of acetylated α-tubulin staining at the apical cell surface (unpublished data), indicative of defective ciliogenesis.

As cilia staining with acetylated α-tubulin antibody did not permit reliable, quantitative measures, we performed scanning EM (SEM) on ALId9 MTECs, which distinguished individual ciliated cells and cilia (Fig. 5 C). As expected, several mature cilia were apparent in WT ciliated cells. In contrast, cilia were scarce in general and appeared stunted at variable levels in CbyKO cultures. We then used SEM images to count the number of cilia per single ciliated cell (Fig. 5 D). The number of cilia per WT cell varied from 80 to 205 with a mean of 147. Conversely, CbyKO ciliated cells showed a significant reduction in the number of cilia per cell ranging from 6 to 155 with a mean of 71. These findings suggest that Cby plays a crucial role in ciliogenesis during airway ciliated cell differentiation.

Cby is required for basal body docking via formation of ciliary vesicles at the distal appendages of nascent centrioles

We previously reported that in nasal and lung bronchial ciliated cells in adult CbyKO mice, although some basal bodies are properly docked with elongated cilia, many basal bodies fail to anchor to the apical membrane and are mispositioned in the apical cytoplasm (Voronina et al., 2009; Love et al., 2010). These observations raised the possibility that Cby plays a role in basal body docking. In agreement with this notion, many basal bodies were located away from the apical cell surface in the tracheal epithelium of adult CbyKO mice (Fig. S5 A). This apparent basal body docking defect was also observed in CbyKO ciliated cells in MTEC cultures through SIM imaging of GFP–centrin-2 and CEP164 (Fig. S5 B). Additionally, an elevated number of stage III ciliated cells in CbyKO MTEC cultures at ALId5 also pointed to defective basal body docking (Fig. 5 B). Collectively, these observations suggest that in the absence of Cby, basal bodies migrate apically but are not able to efficiently anchor to the apical membrane, resulting in an accumulation of basal bodies in the apical cytoplasm.

Once centrioles are fully replicated, small vesicles presumably derived from the Golgi compartment are recruited to the distal appendages and fuse to form a ciliary vesicle that covers the distal end of the centriole (Sorokin, 1968). Although the mechanistic basis of basal body docking remains poorly understood and other mechanisms and models are possible, it is thought that the ciliary vesicle facilitates basal body docking through fusion with the apical plasma membrane. We hypothesized that Cby might be involved in recruitment of vesicles to the distal appendages or subsequent fusion events. In support of this, immuno-EM demonstrated that in differentiating ciliated cells, Cby protein was prominently present at the distal appendages of migrating basal bodies where small vesicles were recruited (Fig. 6 A, arrowheads). Moreover, 3D-SIM imaging of Cby and CEP164 double immunostaining of a stage II ciliated cell showed that Cby initially appeared as single dots and then clustered as rings at the distal end of cytoplasmic basal bodies in close proximity to CEP164 (Video 2).

To directly quantify the number of centrioles bound to membrane vesicles, because of their low abundance and transient nature, tracheas excised from postnatal day 6 (P6) WT and CbyKO mice were cultured for 16 h in the presence of taxol, a microtubule-stabilizing agent, before fixing and processing for EM. In cultured multiciliated cells from the quail oviduct, taxol blocks apical migration of centrioles without overtly affecting centriole replication, resulting in enrichment of centrioles associated with vesicles (Boisvieux-Ulrich et al., 1989). In WT mouse tracheal epithelium, 85% of centrioles were bound to membrane vesicles (89 out of 105 centrioles), whereas only 43% were associated with vesicles in CbyKO ciliated cells (45 out of 105 centrioles; Fig. 6 B). To our surprise, in WT cells, we occasionally observed clusters of cilia that had grown intracellularly (Fig. 6 C). These cytoplasmic cilia had a typical 9+2 pattern of axonemal microtubules, which were surrounded by the ciliary membrane extending from the distal appendages (Fig. 6 C, WT arrowheads). Conversely, in CbyKO ciliated cells, albeit less electron-dense, elongated axonemes devoid of ciliary membranes were seen in the cytoplasm (Fig. 6 C, KO yellow arrowheads), but centrioles were attached to only small vesicles at best (Fig. 6 C, KO white arrowheads), and extended ciliary membranes were absent. We also noted that undocked basal bodies in airway ciliated cells from CbyKO mice are typically associated with no or only small vesicles (unpublished data). These data imply that Cby may play a role in formation of ciliary vesicles at the distal appendages.

Cby coordinates the timing of Rab8 recruitment and basal body docking

Docking of small membrane vesicles at the distal appendages of mother centrioles marks the onset of ciliary vesicle/membrane formation (Rohatgi and Snell, 2010; Westlake et al., 2011; Schmidt et al., 2012). During assembly of primary cilia, the small GTPases Rab11 and Rab8 and the Rab8 GEF Rabin8 play crucial roles in vesicle transport and fusion to facilitate ciliary membrane biogenesis (Nachury et al., 2007; Westlake et al., 2011; Feng et al., 2012; Chiba et al., 2013). Rab11 directly binds to Rabin8 and stimulates its GEF activity, leading to

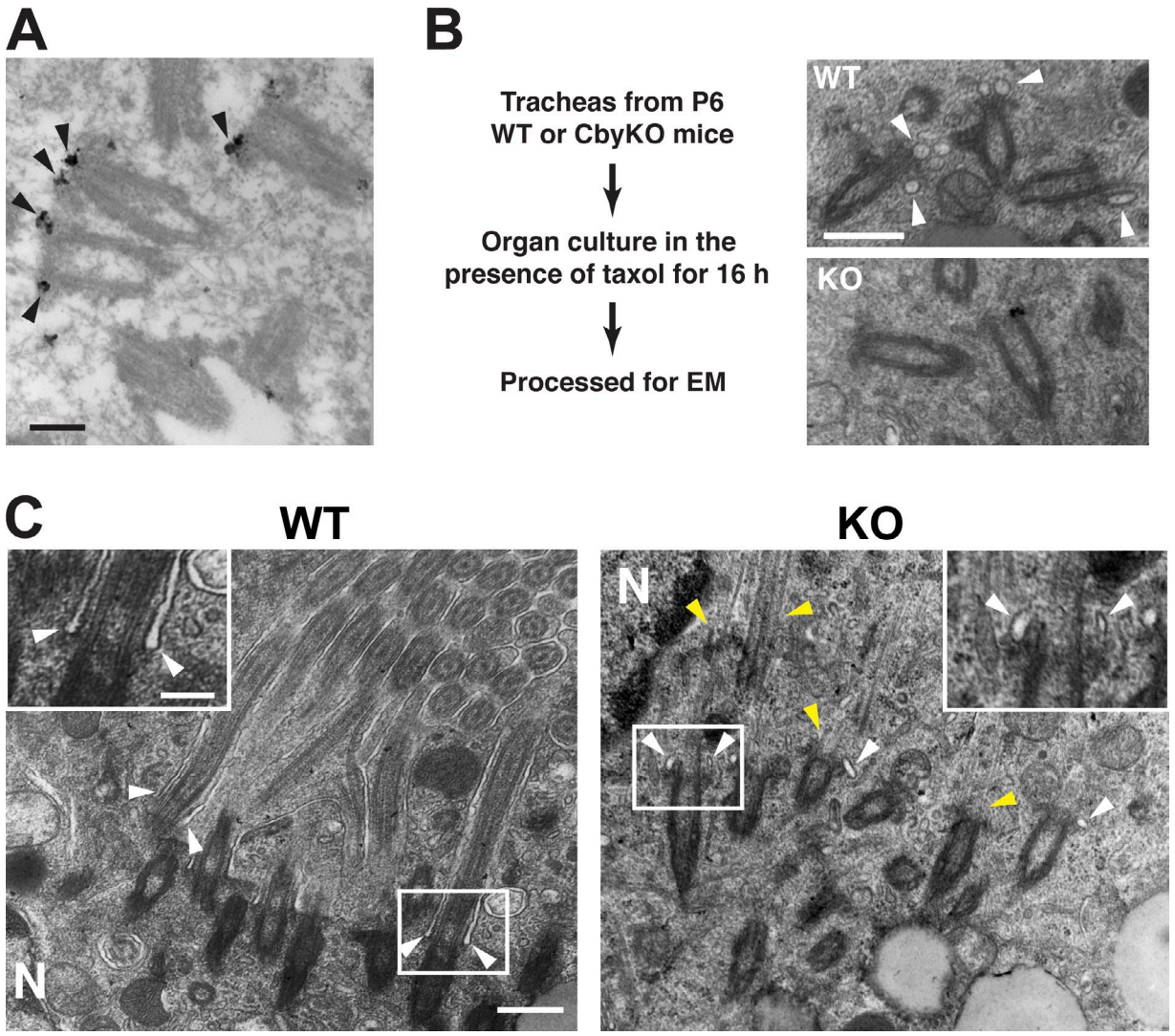

Figure 6. **Diminished recruitment of vesicles to the distal appendages in CbyKO ciliated cells.** (A) Immuno-EM localization of Cby in early ciliated cell differentiation in MTEC cultures. Cby protein (arrowheads) localizes to the distal appendages of migrating basal bodies in the cytoplasm. See also Video 2. (B) Tracheal explants from P6 WT and CbyKO mice were cultured in the presence of taxol for 16 h to enrich vesicle-bound centrioles and processed for EM. Representative EM images are shown. Centrioles attached to vesicles (arrowheads) were more abundant in WT than CbyKO ciliated cells. (C) EM images of ciliated cells from taxol-treated P6 tracheas. The squared areas are shown in higher magnification at the top corners. In WT, cilium growth was occasionally observed in the cytoplasm, with ciliary membrane originating from the distal appendages (arrowheads). Although extended axonemal microtubules were present in CbyKO (yellow arrowheads), elongated ciliary membrane was not noticeable, but instead, centrioles were associated with small vesicles (white arrowheads). N, nucleus. Bars: (A and C, insets) 0.2 µm; (B and C, main images) 0.5 µm.

recruitment and local activation of Rab8 and subsequent delivery and docking of secretory vesicles to the ciliary membrane. Recently, CEP164 has been shown to interact with Rabin8 and recruit Rab8 vesicles to mediate vesicular docking to the distal appendages of mother centrioles during early phases of primary ciliogenesis (Schmidt et al., 2012).

To explore the potential involvement of Cby in vesicle trafficking during airway ciliated cell differentiation, we first examined Rab8 localization in MTEC cultures. In WT ciliated cells, massive enrichment of Rab8 near the apical cell surface was typically apparent when γ-tubulin–positive basal bodies approached the apical membrane at stage III (Fig. 7 A) but rarely observed at stage II when centrioles were still replicating (Fig. 7 B). However, in CbyKO ciliated cells, we noticed precocious accumulation of Rab8 in the apical region at stage II (Fig. 7, A and B). We found no appreciable differences in protein levels of Rab8 and Rabin8 between WT and CbyKO MTECs at ALId0, d5, and d14 (Fig. 7 C). Thus, we interpreted these results to indicate that the defective ciliary vesicle formation in CbyKO ciliated cells might be attributable, at least in part, to a failure of timely recruitment of Rab8 to centrioles before basal body docking, causing precocious apical targeting of Rab8.

To gain insights into the molecular basis of Rab8 recruitment by Cby, we sought to determine whether Cby forms a complex with any of the ciliary membrane trafficking machinery components using co-IP assays. As shown in Fig. 7 D, specific interactions between Cby and Rabin8 were detected. Neither Rab8a (WT Rab8a, GTP-locked Rab8a-Q67L, and

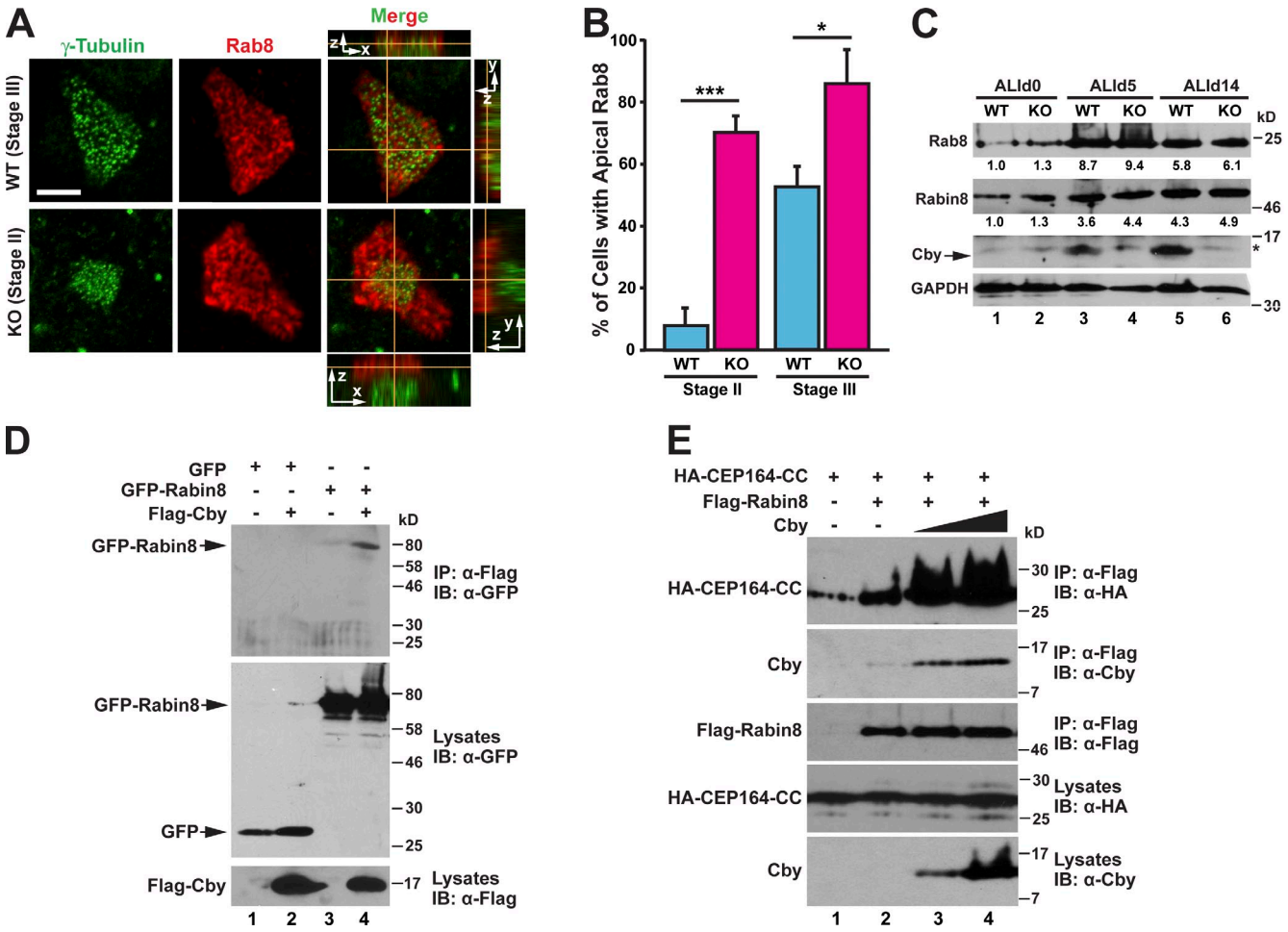

Figure 7. **Cby facilitates recruitment of Rab8 to the basal bodies via stabilization of the CEP164–Rabin8 complex.** (A) MTECs were fixed at ALId4 and immunostained for γ-tubulin and Rab8. Top-down (x-y) and side (y-z on the right and x-z on the top or bottom) views are shown. Bar, 5 µm. (B) Quantification of the number of ciliated cells with apical Rab8 at the indicated ciliogenesis stages. MTECs were fixed at ALId3 through d6 and colabeled with γ-tubulin and Rab8 antibodies. For each genotype, 51–108 ciliated cells were counted per MTEC preparation, and data are presented as means ± SEM from four independent MTEC preparations. *, $P < 0.05$; ***, $P < 0.001$. (C) Cell lysates were prepared from WT or CbyKO MTECs at ALId0, d5, and d14 and subjected to Western blotting for Rab8, Rabin8, Cby, and GAPDH as indicated. The asterisk indicates a nonspecific band. The band intensities of Rab8 and Rabin8 were quantified and normalized to those of GAPDH. The normalized values for WT samples at ALId0 were set as 1. (D) HEK293T cells were transfected with GFP or GFP-Rabin8 and Flag-Cby expression plasmids as shown, and cell lysates were immunoprecipitated with the Flag antibody and probed with the GFP antibody. (E) Cell lysates were prepared from HEK293T cells expressing HA–CEP164-CC, Flag-Rabin8, and increasing amounts of untagged Cby, which was immunoprecipitated with the Flag antibody and detected with the HA, Cby, or Flag antibody as shown. IB, immunoblot; IP, immunoprecipitation.

GDP-locked Rab8a-T22N) nor Rab11a (WT Rab11a and GDP-locked Rab11a-S25N) bound to Cby (unpublished data). Because Cby binds to the same C-terminal domain of CEP164 as Rabin8 does (Schmidt et al., 2012), we considered the possibility that Cby might influence CEP164–Rabin8 interactions. To test this, we cotransfected a constant amount of expression plasmids for HA–CEP164-CC and Flag-Rabin8 and increasing amounts of an untagged Cby plasmid into HEK293T cells for co-IP assays using the Flag antibody. Elevated levels of CEP164 were precipitated with Rabin8 upon Cby expression in a dose-dependent manner (Fig. 7 E). Collectively, these data suggest that Cby facilitates CEP164 association with Rabin8, leading to efficient recruitment and activation of Rab8 at the distal appendages of centrioles to promote ciliary vesicle formation and subsequent basal body docking.

Discussion

A model for basal body docking

Since the first morphological EM study on differentiating ciliated cells in rat lungs in the 1960s (Sorokin, 1968), the molecular basis for basal body docking has remained largely elusive. Here, we demonstrated that Cby is required for proper docking of basal bodies to apical membranes in differentiating airway ciliated cells. We propose the following model for the role of Cby in this process (Fig. 8). Upon replication of centrioles, the distal appendage protein CEP164 physically binds and recruits Cby in a ring-shaped pattern at the distal end of centrioles. Cby then interacts with Rabin8 and enhances the formation of the CEP164 and Rabin8 complex, thereby promoting recruitment and local activation of Rab8 as centrioles migrate apically. This

leads to polarized transport and fusion of Rab8-positive vesicles to ensure maturation of ciliary vesicles, enabling robust basal body docking to the apical membrane. Cby continues to localize at the ciliary base of elongating and mature cilia, suggesting that Cby is also involved in biogenesis and homeostasis of the ciliary membrane. Although Cby and CEP164 show substantial overlapping distribution (Figs. 3 B and S3), the fact that Cby rings are slightly smaller in diameter than and located distally to CEP164 rings suggests that the Cby–CEP164 interaction is transient and dynamically regulated, and Cby is recruited to the transition fibers initially by CEP164 and may travel inward and upward into the transition zone independently of CEP164. In CbyKO ciliated cells, CEP164 localization is unaffected, but Rab8 trafficking to the distal appendages is severely compromised. Rab8 vesicles are instead targeted to the apical cell surface, thereby inhibiting proper ciliary vesicle formation and basal body docking. Our finding that no primary cilia are observed in CbyKO MTEC cultures at ALId2 (Fig. 5 A) suggests that this mechanism also operates during primary ciliogenesis.

We also noticed that there is a consistent decrease in the number of Foxj1-positive cells in CbyKO MTEC cultures at all stages examined in comparison with WT MTEC cultures (Fig. S4). This could be explained, at least in part, by the lack of primary cilia in CbyKO MTECs at early differentiation stages (Fig. 5 A). Airway progenitor cells possess primary cilia, and it has been proposed that primary cilia play critical roles in differentiation of multiciliated cells (Jain et al., 2010). Thus, the loss of primary cilia might be a contributing factor to defective ciliated cell differentiation in CbyKO MTECs.

Physiological significance of ciliary vesicles in basal body docking

The physiological role of ciliary vesicles is poorly understood, although their morphology in both primary and multiciliated cells was first described in the 1960s (Sorokin, 1962, 1968). Once fully formed, these ciliary vesicles seem to flatten and later fuse with the apical plasma membrane (Sorokin, 1968). Our study highlights for the first time, to our knowledge, their biological importance for appropriate basal body docking. It should be noted that in the absence of Cby, some basal bodies succeed in anchoring to the apical cell surface and extending apparently normal cilia (Fig. 5 C; Voronina et al., 2009; Love et al., 2010). In this scenario, albeit less efficiently, basal bodies with no or incomplete ciliary vesicles are probably capable of finding their way to dock to the apical membrane. Accordingly, Cby as well as ciliary vesicles are most likely dispensable for the migration and docking events per se but are necessary for efficient basal body docking. We speculate that the ciliary vesicle system is of particular importance for the orchestration of differentiation and ciliogenesis of multiciliated cells as they coordinate the docking of hundreds of basal bodies over a short period of time.

Cby localization in airway ciliated cells

Throughout differentiation of MTECs, Cby localizes to the centrioles/basal bodies (Fig. 1 A). We also detected Cby-positive acentriolar areas that colocalize with IFT20 in early differentiation stages (Fig. 1 B). The number and size of these structures are variable, and

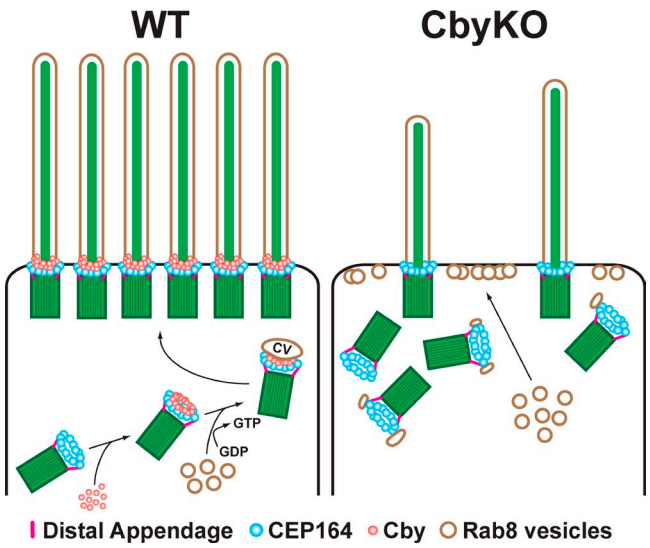

Figure 8. **Model for basal body docking during airway ciliated cell differentiation.** Upon centriole replication, CEP164 recruits Cby to the distal appendages. Cby in turn promotes efficient recruitment and fusion of Rab8-positive vesicles to form a ciliary vesicle at the distal end of centrioles. This facilitates docking of basal bodies to the apical membrane. In the absence of Cby, ciliary vesicles fail to form as a result of the inability to recruit sufficient Rab8 vesicles, resulting in compromised basal body docking. CV, ciliary vesicle. See Discussion for details.

they seem to appear only transiently. At present, their exact identity is unknown, but they bear resemblance to fibrogranular areas observed by EM in immature ciliated cells, which are considerably larger than deuterosomes and thought to contain precursor materials from which multiple deuterosomes arise (Sorokin, 1968). Although it remains fully speculative at the moment, it is possible that at least some centrosomal proteins are already transported to discrete domains in the apical cytoplasm, destined to produce deuterosomes before procentriole formation.

Using superresolution microscopy, we found that Cby molecules cluster at the base of cilia as a ring with a diameter of 300 nm and a height of 100 nm (Fig. 3 D). Notably, immuno-EM revealed that Cby is most abundant around the distal portion of the transition fibers, where these fibers contact the apical membrane (Fig. 3 C). Worthy of note, the anterograde IFT component IFT52 has been shown to localize around the periphery of the transition fibers in *Chlamydomonas reinhardtii* (Deane et al., 2001). These findings reinforce the idea that the transition fibers, which demarcate the entrance to the ciliary compartment, constitute docking and releasing sites for various ciliary cargo particles and vesicles (Deane et al., 2001). Cby was also detected in the proximal region of the transition zone, slightly apical to the transition fibers (Fig. 3 C). There, Cby localizes near the ciliary membrane, consistent with our model that Cby is involved in biogenesis of ciliary vesicles/membranes.

During migration of centrioles, Cby localizes to the distal appendages where ciliary vesicles assemble (Fig. 6 A). In CbyKO ciliated cells, distal appendages seem to be structurally and functionally normal as they are able to capture small vesicles (Fig. 6 C), indicating that Cby is not a structural component of the distal appendages and that its distribution is likely to be dynamically regulated.

Molecular network for ciliary vesicle biosynthesis

The molecular mechanisms and components for ciliary vesicle formation are beginning to emerge. In RPE1 cells, CEP164 has recently been shown to be required for initial attachment of vesicles to the distal appendages of mother centrioles upon induction of ciliogenesis (Schmidt et al., 2012). Although the mechanistic details of vesicle docking are unclear, CEP164 directly interacts with Rabin8, which in turn recruits Rab8 vesicles. Given the fact that in the absence of Cby, initial small vesicles come into contact with the distal appendages (Fig. 6 C), Cby is not essential for the vesicle-distal appendage attachment but is rather required for the subsequent vesicle stabilization or fusion.

Cenexin, an Odf2 variant, is located at the distal and subdistal appendages and plays an essential role for formation of these appendage structures (Ishikawa et al., 2005). Previously, we and others reported that Cenexin is indispensable for Cby centriolar localization (Steere et al., 2012; Chang et al., 2013). More recently, it was shown that in F9 cells devoid of Cenexin, CEP164 and Cby fail to localize to the mother centriole, suggesting that Cenexin lies upstream of CEP164 and Cby in this assembly pathway (Tateishi et al., 2013). CEP123 (also known as CEP89) and CCDC41 are essential ciliogenesis factors that reside at the distal end of mother centrioles, and their siRNA-mediated knockdown is associated with altered ciliary vesicle formation in RPE1 cells (Joo et al., 2013; Sillibourne et al., 2013). Interestingly, CEP164 localizes to the distal appendages independently of CEP123 and CCDC41, indicative of the existence of distinct modular complexes (Joo et al., 2013; Sillibourne et al., 2013; Tanos et al., 2013). A recent study, using quantitative centrosome proteomics, identified the novel distal appendage components CEP83, SCLT1, and FBF1 (Tanos et al., 2013). It will be of importance in future studies to decipher the molecular nature of protein–protein interactions and how these factors contribute to the assembly of distal appendages and ciliary vesicles.

In summary, our study reveals that Cby acts in basal body docking by promoting proper formation of ciliary vesicles. Cby interacts with CEP164 and Rabin8 and promotes stabilization or fusion of small vesicles at the distal appendages to assemble a ciliary vesicle. Our findings underscore the critical role of ciliary vesicles in basal body docking during the differentiation of airway ciliated cells.

Materials and methods

Mouse strains

The CbyKO mouse line was generated by replacing the entire coding region with a neomycin cassette as previously described (Voronina et al., 2009), and they were maintained on a mixed C57BL/6J and 129/SvJ background. Transgenic mice expressing GFP–centrin-2 under the control of a cytomegalovirus immediate-early enhancer/β-actin promoter (Higginbotham et al., 2004) were purchased from The Jackson Laboratory. Cby heterozygous mice were crossed with GFP–centrin-2 mice to generate cohorts of WT and CbyKO mice carrying the GFP–centrin-2 transgene. All mice were handled according to National Institutes of Health guidelines, and all experimental procedures were approved by the Institutional Animal Care and Use Committee of the Stony Brook University and National Jewish Health.

Naphthalene-induced airway injury and morphometry

Adult WT and CbyKO mice were treated intraperitoneally with 300 mg/kg naphthalene (Thermo Fisher Scientific) dissolved in Mazola corn oil and recovered for 13 d. Lungs were inflation fixed with 4% PFA, paraffin embedded, sectioned at 5 µm, and immunostained with antibodies against acetylated α-tubulin (mouse; Sigma-Aldrich) and Clara cell secretary protein (CCSP; goat; Stripp et al., 2002). Nuclei were visualized with DAPI. Three to four bronchiolar regions from each of five mice/genotype/treatment were imaged at 200×. Stereological methods were used to calculate the volume density or fraction of cell markers (Vv) and the surface area of the epithelial basement membrane per reference volume (Sv; Cole et al., 2010; Hsia et al., 2010). Vv was determined by counting test points (P) using a grid of evenly spaced points and was calculated by the formula $V_V = P_N/P_T$. Hence, Vv was determined by counting the number of points intersecting the structure of interest (P_N) divided by the total points intersecting the reference space (P_T). The structures of interest were nuclei defined by DAPI staining, ciliated cells defined by staining for acetylated α-tubulin, and Clara cells defined by CCSP expression. The reference space was the epithelium defined by autofluorescence. S_V was determined by counting intercepts (I) between the surface and grid of evenly spaced cycloid lines and was calculated using the formula $S_V = 2I_0/Lr$. I_0 was the number of intersections between the cycloid grid and a surface, the basement membrane. Lr was the total length of the test line within the reference volume, the epithelium. 2 was the constant. The volume densities of cell markers within the epithelial compartment per surface area of basal lamina were calculated using the formula $V_S = V_V/S_V$.

Measurement of cilia-generated flow and directionality and ex vivo culture of tracheas

To quantify cilia-generated flow and directionality across the luminal surface of tracheas, freshly excised adult tracheas were cut open longitudinally and placed in Ham's F-12 medium supplemented with 5% FBS. Red fluorescent carboxylate-modified polystyrene microspheres (0.5 µm; Sigma-Aldrich) were added to the medium, and the movement of the microspheres was recorded at 10 frames per second using a charge-coupled device (CCD) camera (MDC140BW; ScopeTek) on a microscope (Axio Examiner.A1; Carl Zeiss) with a 40× objective. Flow rates and directionality were calculated as previously described (Park et al., 2008). Flow rates were quantified as the net linear distance of individual bead tracks from the distal to the proximal trachea per minute. Directionality was defined as the ratio of the linear distance between the first and last points of a track and the total distance along the track.

For quantification of centrioles attached to vesicles, freshly harvested tracheas from P6 mice (three/genotype) were cultured in a 5% CO_2 atmosphere for 16 h at 37°C in DMEM with 10% FBS, 1 µg/ml insulin, 30 ng/ml dexamethasone, and 100 U/ml penicillin-streptomycin in the presence of 1 µM paclitaxel (Enzo Life Sciences) and then processed for EM. Centrioles with or without vesicles in longitudinal orientation were counted on EM images.

Plasmids and reagents

Expression constructs for pCS2+Flag-Cby (Li et al., 2008), pCS2+Flag–Cby-4A (Mofunanya et al., 2009), a cytomegalovirus-driven expression plasmid for 3×HA-CEP164 (gift from H.H. Arts, Radboud University, Nijmegen, Netherlands and F. Hildebrandt, Harvard Medical School, Boston, MA; Chaki et al., 2012), and pEGFP-C–EGFP-Rabin8 (Westlake et al., 2011) have been described previously. For generation of HA-tagged human CEP164 deletion and Rab8a and Rab11a constructs, corresponding inserts were amplified by PCR and subcloned into pCS2+HA. Similarly, cDNAs for Cby-N (aa 1–63), Cby-C (aa 64–126), Rabin8, and EGFP were amplified by PCR and subcloned into pCS2+Flag. Lentiviral expression constructs for Flag-tagged human Cby-FL, -C (aa 49–126), and -4A were created by inserting PCR-amplified cDNAs into a second generation lentiviral transfer vector pEF1α–internal ribosome entry site–EGFP (gift from I. Lemischka, Mount Sinai Medical Center, New York, NY). Lentiviruses were produced by transient transfection of HEK293T cells according to standard protocols. All chemicals were purchased from Sigma-Aldrich unless otherwise noted.

Cell culture, transfection, MTEC preparation, and lentiviral infection

HEK293T, U2OS, and GFP–centrin-1–expressing HeLa (Steere et al., 2012) cells were maintained in DMEM or DMEM-GlutaMAX with 10% FBS and 100 U/ml penicillin-streptomycin. Transfections were performed using ExpressFect (Denville Scientific).

For RNAi knockdown of CEP164, HeLa, U2OS, and RPE1, cells seeded on coverslips in a 12-well plate were transfected with or without 40 pmol siRNA duplexes using Lipofectamine 2000 (Invitrogen) according to the manufacturer's instructions. RPE1 cells were serum starved for 48 h to induce ciliation. The target sequence corresponds to human CEP164 at

nucleotide positions 2,381–2,399 (5′-GAAGATACAGGAAGCTCAA-3′), which is tagged with dTdT overhang at the 3′ terminus (Sigma-Aldrich).

In vitro cultures of MTECs were established on membranes using ALI conditions as described previously (You et al., 2002). In brief, tracheas were excised from 2–6-mo-old WT and CbyKO mice, and epithelial cells were harvested by pronase digestion, seeded onto Transwell polycarbonate or polyester permeable membranes (6.5-mm diameter; Corning), and proliferated to confluence in growth media. Subsequently, the ALI was created by removing apical chamber media and switching in the lower compartment to differentiation media with 2% NuSerum (BD). For viral infection of MTECs, isolated epithelial cells were mixed with lentiviral supernatants in the presence of 10 µg/ml protamine sulfate (Sigma-Aldrich) at the time of seeding.

Confocal and superresolution microscopy

MTECs on supported membranes were fixed in either 3.2% PFA/3% sucrose in PBS, pH 7.4, or methanol-acetone (1:1), depending on antigen (Table S1), cut from supports into quarters, and processed for immunostaining as previously described (You et al., 2002). HeLa and U2OS cells were fixed with methanol. The fixed samples were incubated with primary antibodies overnight at 4°C followed by secondary antibodies conjugated with DyLight 488, DyLight 549, or Cy5 fluorescent dyes (Jackson ImmunoResearch Laboratories, Inc.). All primary antibodies used are listed in Table S1. Alexa Fluor 488–conjugated lectin HPA was obtained from Molecular Probes. Labeled samples were stained with DAPI before mounting with Fluoromount-G (SouthernBiotech). Samples were viewed at room temperature with a confocal microscope (LSM 510; Carl Zeiss) with a 63×/1.4 NA or a 100×/1.4 NA objective. Images were acquired using a digital camera (AxioCam MRm; Carl Zeiss) with AxioVision software (Carl Zeiss). For SIM imaging, specimens were analyzed by an N-SIM (Nikon) with a 100×/1.49 NA objective. For direct STORM imaging, methanol-acetone–fixed MTECs were incubated with Cby8-2 antibody and then with Alexa Fluor 647 anti–mouse IgG secondary antibody (Molecular Probes) and imaged at room temperature by an N-STORM (Nikon) with a 100×/1.49 NA objective using a buffer containing cysteamine as the thiol source (Laevsky and O'Connell, 2013). N-SIM and N-STORM were equipped with electron-multiplying CCD cameras (iXon3 897 and Ultra 897, respectively; Andor Technology) with NIS-Elements image analysis software (Nikon).

EM, immuno-EM, and SEM

EM and SEM were performed by standard methods as previously described (Voronina et al., 2009; Love et al., 2010). For EM, tracheas were fixed in 2% PFA and 2% glutaraldehyde, postfixed in 2% osmium tetroxide, dehydrated, and embedded in Durcupan resin. Ultrathin sections of 80 nm were cut with an ultramicrotome (Ultracut E; Reichert–Jung) and placed on formvar-coated slot copper grids. Sections were then counterstained with uranyl acetate and lead citrate and imaged by an electron microscope (Tecnail2 BioTwinG2; FEI) with a CCD digital camera system (XR-60; Advanced Microscopy Techniques). Preembedding immuno-EM of Cby localization was adapted from Hagiwara et al. (2010). MTECs were fixed with 4% PFA and 0.2% glutaraldehyde, permeabilized with 0.01% Triton X-100, and incubated with Cby8-2 mouse monoclonal antibody (Cyge et al., 2011) and then with 1.4-nm Nanogold-conjugated anti–mouse IgG secondary antibody (Nanoprobes) followed by postfixation with 2% PFA and 2% glutaraldehyde. The size of gold particles was enhanced using the HQ Silver Enhancement kit (Nanoprobes). The samples were then processed for EM. For SEM, ALId9 MTECs were fixed in 2% PFA and 2% glutaraldehyde, dehydrated, and transferred to 100% hexamethyldisilazane (Electron Microscopy Sciences) through a graded series of ethanol-hexamethyldisilazane mixtures. The specimens were air dried, mounted on a SEM stubs, and sputter coated with gold before examination with a scanning electron microscope (LEO 1550; Carl Zeiss) at 10 kV using a back scatter detector (Robinson).

Co-IP and Western blotting

Co-IP and immunoblotting were performed as previously described (Li et al., 2008, 2010). In brief, transfected HEK293T cells were harvested in ice-cold lysis buffer (20 mM Tris-HCl, pH 8.0, 135 mM NaCl, 1.5 mM $MgCl_2$, 1 mM EGTA, 1% Triton X-100, and 10% glycerol) with protease inhibitor cocktail (Sigma-Aldrich) and incubated for 20 min on ice with intermittent agitation. Cell lysates were cleared by centrifugation at 12,000 rpm for 30 min at 4°C. The supernatants were then incubated with 1 µg of primary antibody as indicated for 1 h at 4°C followed by the addition of protein A/G beads (Sigma-Aldrich) and rotation for 1 h. The beads were collected and washed twice with 1 ml of ice-cold lysis buffer before SDS-PAGE. The primary antibodies used were as follows: mouse Flag M2 (Sigma-Aldrich), rat HA (Roche), rabbit GFP (generated through GE Healthcare), rabbit CEP164 (Sigma-Aldrich), rabbit Rab8a (Proteintech), rabbit Rabin8 (Proteintech), rabbit Cby (Takemaru et al., 2003), rabbit Cby (Proteintech), and mouse GAPDH (Meridian Life Science). Relative band intensities on Western blots were quantified using ImageJ (National Institutes of Health).

Statistical analysis

Two-tailed Student's *t* test was used for data analysis. In the figures, asterisks indicate p-values as follows: *, $P < 0.05$; **, $P < 0.01$; ***, $P < 0.001$; and ****, $P < 0.0001$.

Online supplemental material

Fig. S1 shows a paucity of cilia and impaired mucociliary transport in the airways of CbyKO mice. Fig. S2 shows the localization of Cby in relation to centrin and Golgi markers in ciliated cells. Fig. S3 shows SIM imaging of Cby and CEP164 in ciliated cells. Fig. S4 provides quantification of Foxj1-positive cells in MTEC cultures. Fig. S5 shows basal body docking defects in tracheal ciliated cells in CbyKO mice. Table S1 lists antibodies used for immunofluorescence microscopy. Video 1 shows z-stack SIM images of Cby and cilia in ciliated cells. Video 2 shows z-stack SIM images of Cby and CEP164 in a stage II ciliated cell. Online supplemental material is available at http://www.jcb.org/cgi/content/full/jcb.201406140/DC1. Additional data are available in the JCB DataViewer at http://dx.doi.org/10.1083/jcb.201406140.dv.

We thank S.L. Brody, G.J. Pazour, E.A. Nigg, G. Pereira, H.H. Arts, and F. Hildebrandt for reagents, S. Ge for the use of microscopes, S. Van Horn from the Central Microscopy Center and J. Quinn for technical assistance with EM and SEM, respectively, and M. Kernan for critical reading of the manuscript.

This work was supported by a National Science Foundation grant (MCB1140033) to R. Kuriyama, an American Heart Association Grant-in-Aid (11GRNT7860023) to F.-Q. Li, and a National Institutes of Health/National Heart, Lung, and Blood Institute grant (R01HL107493) to K.-I. Takemaru.

The authors declare no competing financial interests.

Submitted: 30 June 2014
Accepted: 9 September 2014

References

Blatt, E.N., X.H. Yan, M.K. Wuerffel, D.L. Hamilos, and S.L. Brody. 1999. Forkhead transcription factor HFH-4 expression is temporally related to ciliogenesis. *Am. J. Respir. Cell Mol. Biol.* 21:168–176. http://dx.doi.org/10.1165/ajrcmb.21.2.3691

Boisvieux-Ulrich, E., M.C. Laine, and D. Sandoz. 1989. In vitro effects of taxol on ciliogenesis in quail oviduct. *J. Cell Sci.* 92:9–20.

Chaki, M., R. Airik, A.K. Ghosh, R.H. Giles, R. Chen, G.G. Slaats, H. Wang, T.W. Hurd, W. Zhou, A. Cluckey, et al. 2012. Exome capture reveals ZNF423 and CEP164 mutations, linking renal ciliopathies to DNA damage response signaling. *Cell*. 150:533–548. http://dx.doi.org/10.1016/j.cell.2012.06.028

Chang, J., S.G. Seo, K.H. Lee, K. Nagashima, J.K. Bang, B.Y. Kim, R.L. Erikson, K.W. Lee, H.J. Lee, J.E. Park, and K.S. Lee. 2013. Essential role of Cenexin1, but not Odf2, in ciliogenesis. *Cell Cycle*. 12:655–662. http://dx.doi.org/10.4161/cc.23585

Chiba, S., Y. Amagai, Y. Homma, M. Fukuda, and K. Mizuno. 2013. NDR2-mediated Rabin8 phosphorylation is crucial for ciliogenesis by switching binding specificity from phosphatidylserine to Sec15. *EMBO J.* 32:874–885. http://dx.doi.org/10.1038/emboj.2013.32

Cole, B.B., R.W. Smith, K.M. Jenkins, B.B. Graham, P.R. Reynolds, and S.D. Reynolds. 2010. Tracheal Basal cells: a facultative progenitor cell pool. *Am. J. Pathol.* 177:362–376. http://dx.doi.org/10.2353/ajpath.2010.090870

Cyge, B., V. Fischer, K. Takemaru, and F.Q. Li. 2011. Generation and characterization of monoclonal antibodies against human Chibby protein. *Hybridoma (Larchmt)*. 30:163–168. http://dx.doi.org/10.1089/hyb.2010.0098

Czarnecki, P.G., and J.V. Shah. 2012. The ciliary transition zone: from morphology and molecules to medicine. *Trends Cell Biol.* 22:201–210. http://dx.doi.org/10.1016/j.tcb.2012.02.001

Dawe, H.R., H. Farr, and K. Gull. 2007. Centriole/basal body morphogenesis and migration during ciliogenesis in animal cells. *J. Cell Sci.* 120:7–15. http://dx.doi.org/10.1242/jcs.03305

Deane, J.A., D.G. Cole, E.S. Seeley, D.R. Diener, and J.L. Rosenbaum. 2001. Localization of intraflagellar transport protein IFT52 identifies basal body transitional fibers as the docking site for IFT particles. *Curr. Biol.* 11:1586–1590. http://dx.doi.org/10.1016/S0960-9822(01)00484-5

Dirksen, E.R. 1991. Centriole and basal body formation during ciliogenesis revisited. *Biol. Cell*. 72:31–38. http://dx.doi.org/10.1016/0248-4900(91)90075-X

Enjolras, C., J. Thomas, B. Chhin, E. Cortier, J.L. Duteyrat, F. Soulavie, M.J. Kernan, A. Laurençon, and B. Durand. 2012. *Drosophila chibby* is required for basal body formation and ciliogenesis but not for Wg signaling. *J. Cell Biol.* 197:313–325. http://dx.doi.org/10.1083/jcb.201109148

Feng, S., A. Knödler, J. Ren, J. Zhang, X. Zhang, Y. Hong, S. Huang, J. Peränen, and W. Guo. 2012. A Rab8 guanine nucleotide exchange factor-effector interaction network regulates primary ciliogenesis. *J. Biol. Chem.* 287:15602–15609. http://dx.doi.org/10.1074/jbc.M111.333245

Follit, J.A., R.A. Tuft, K.E. Fogarty, and G.J. Pazour. 2006. The intraflagellar transport protein IFT20 is associated with the Golgi complex and is required for cilia assembly. *Mol. Biol. Cell*. 17:3781–3792. http://dx.doi.org/10.1091/mbc.E06-02-0133

Goetz, S.C., and K.V. Anderson. 2010. The primary cilium: a signalling centre during vertebrate development. *Nat. Rev. Genet.* 11:331–344. http://dx.doi.org/10.1038/nrg2774

Graser, S., Y.D. Stierhof, S.B. Lavoie, O.S. Gassner, S. Lamla, M. Le Clech, and E.A. Nigg. 2007. Cep164, a novel centriole appendage protein required for primary cilium formation. *J. Cell Biol.* 179:321–330. http://dx.doi.org/10.1083/jcb.200707181

Hagiwara, H., T. Aoki, T. Suzuki, and K. Takata. 2010. Pre-embedding immunoelectron microscopy of chemically fixed mammalian tissue culture cells. *Methods Mol. Biol.* 657:145–154. http://dx.doi.org/10.1007/978-1-60761-783-9_11

Higginbotham, H., S. Bielas, T. Tanaka, and J.G. Gleeson. 2004. Transgenic mouse line with green-fluorescent protein-labeled Centrin 2 allows visualization of the centrosome in living cells. *Transgenic Res.* 13:155–164. http://dx.doi.org/10.1023/B:TRAG.0000026071.41735.8e

Hildebrandt, F., T. Benzing, and N. Katsanis. 2011. Ciliopathies. *N. Engl. J. Med.* 364:1533–1543. http://dx.doi.org/10.1056/NEJMra1010172

Hsia, C.C., D.M. Hyde, M. Ochs, and E.R. Weibel; ATS/ERS Joint Task Force on Quantitative Assessment of Lung Structure. 2010. An official research policy statement of the American Thoracic Society/European Respiratory Society: standards for quantitative assessment of lung structure. *Am. J. Respir. Crit. Care Med.* 181:394–418. http://dx.doi.org/10.1164/rccm.200809-1522ST

Ishikawa, H., A. Kubo, S. Tsukita, and S. Tsukita. 2005. Odf2-deficient mother centrioles lack distal/subdistal appendages and the ability to generate primary cilia. *Nat. Cell Biol.* 7:517–524. http://dx.doi.org/10.1038/ncb1251

Jain, R., J. Pan, J.A. Driscoll, J.W. Wisner, T. Huang, S.P. Gunsten, Y. You, and S.L. Brody. 2010. Temporal relationship between primary and motile ciliogenesis in airway epithelial cells. *Am. J. Respir. Cell Mol. Biol.* 43:731–739. http://dx.doi.org/10.1165/rcmb.2009-0328OC

Joo, K., C.G. Kim, M.S. Lee, H.Y. Moon, S.H. Lee, M.J. Kim, H.S. Kweon, W.Y. Park, C.H. Kim, J.G. Gleeson, and J. Kim. 2013. CCDC41 is required for ciliary vesicle docking to the mother centriole. *Proc. Natl. Acad. Sci. USA*. 110:5987–5992. http://dx.doi.org/10.1073/pnas.1220927110

Klos Dehring, D.A., E.K. Vladar, M.E. Werner, J.W. Mitchell, P. Hwang, and B.J. Mitchell. 2013. Deuterosome-mediated centriole biogenesis. *Dev. Cell*. 27:103–112. http://dx.doi.org/10.1016/j.devcel.2013.08.021

Laevsky, G.S., and C.B. O'Connell. 2013. Comparative and practical aspects of localization-based super-resolution imaging. *Curr. Protoc. Cytom.* Chapter 2:Unit 2.20.

Lau, L., Y.L. Lee, S.J. Sahl, T. Stearns, and W.E. Moerner. 2012. STED microscopy with optimized labeling density reveals 9-fold arrangement of a centriole protein. *Biophys. J.* 102:2926–2935. http://dx.doi.org/10.1016/j.bpj.2012.05.015

Li, F.Q., A. Mofunanya, K. Harris, and K. Takemaru. 2008. Chibby cooperates with 14-3-3 to regulate β-catenin subcellular distribution and signaling activity. *J. Cell Biol.* 181:1141–1154. http://dx.doi.org/10.1083/jcb.200709091

Li, F.Q., A. Mofunanya, V. Fischer, J. Hall, and K. Takemaru. 2010. Nuclear-cytoplasmic shuttling of Chibby controls beta-catenin signaling. *Mol. Biol. Cell*. 21:311–322. http://dx.doi.org/10.1091/mbc.E09-05-0437

Love, D., F.Q. Li, M.C. Burke, B. Cyge, M. Ohmitsu, J. Cabello, J.E. Larson, S.L. Brody, J.C. Cohen, and K. Takemaru. 2010. Altered lung morphogenesis, epithelial cell differentiation and mechanics in mice deficient in the Wnt/β-catenin antagonist Chibby. *PLoS ONE*. 5:e13600. http://dx.doi.org/10.1371/journal.pone.0013600

Mahvi, D., H. Bank, and R. Harley. 1977. Morphology of a naphthalene-induced bronchiolar lesion. *Am. J. Pathol.* 86:558–572.

Mofunanya, A., F.Q. Li, J.C. Hsieh, and K. Takemaru. 2009. Chibby forms a homodimer through a heptad repeat of leucine residues in its C-terminal coiled-coil motif. *BMC Mol. Biol.* 10:41. http://dx.doi.org/10.1186/1471-2199-10-41

Nachury, M.V., A.V. Loktev, Q. Zhang, C.J. Westlake, J. Peränen, A. Merdes, D.C. Slusarski, R.H. Scheller, J.F. Bazan, V.C. Sheffield, and P.K. Jackson. 2007. A core complex of BBS proteins cooperates with the GTPase Rab8 to promote ciliary membrane biogenesis. *Cell*. 129:1201–1213. http://dx.doi.org/10.1016/j.cell.2007.03.053

Nigg, E.A., and J.W. Raff. 2009. Centrioles, centrosomes, and cilia in health and disease. *Cell*. 139:663–678. http://dx.doi.org/10.1016/j.cell.2009.10.036

Park, T.J., B.J. Mitchell, P.B. Abitua, C. Kintner, and J.B. Wallingford. 2008. Dishevelled controls apical docking and planar polarization of basal bodies in ciliated epithelial cells. *Nat. Genet.* 40:871–879. http://dx.doi.org/10.1038/ng.104

Reiter, J.F., O.E. Blacque, and M.R. Leroux. 2012. The base of the cilium: roles for transition fibres and the transition zone in ciliary formation, maintenance and compartmentalization. *EMBO Rep.* 13:608–618. http://dx.doi.org/10.1038/embor.2012.73

Rohatgi, R., and W.J. Snell. 2010. The ciliary membrane. *Curr. Opin. Cell Biol.* 22:541–546. http://dx.doi.org/10.1016/j.ceb.2010.03.010

Rosenbaum, J.L., and G.B. Witman. 2002. Intraflagellar transport. *Nat. Rev. Mol. Cell Biol.* 3:813–825. http://dx.doi.org/10.1038/nrm952

Schmidt, K.N., S. Kuhns, A. Neuner, B. Hub, H. Zentgraf, and G. Pereira. 2012. Cep164 mediates vesicular docking to the mother centriole during early steps of ciliogenesis. *J. Cell Biol.* 199:1083–1101. http://dx.doi.org/10.1083/jcb.201202126

Sillibourne, J.E., C.G. Specht, I. Izeddin, I. Hurbain, P. Tran, A. Triller, X. Darzacq, M. Dahan, and M. Bornens. 2011. Assessing the localization of centrosomal proteins by PALM/STORM nanoscopy. *Cytoskeleton (Hoboken)*. 68:619–627. http://dx.doi.org/10.1002/cm.20536

Sillibourne, J.E., I. Hurbain, T. Grand-Perret, B. Goud, P. Tran, and M. Bornens. 2013. Primary ciliogenesis requires the distal appendage component Cep123. *Biol. Open*. 2:535–545. http://dx.doi.org/10.1242/bio.20134457

Sonnen, K.F., L. Schermelleh, H. Leonhardt, and E.A. Nigg. 2012. 3D-structured illumination microscopy provides novel insight into architecture of human centrosomes. *Biol. Open*. 1:965–976. http://dx.doi.org/10.1242/bio.20122337

Sorokin, S. 1962. Centrioles and the formation of rudimentary cilia by fibroblasts and smooth muscle cells. *J. Cell Biol.* 15:363–377. http://dx.doi.org/10.1083/jcb.15.2.363

Sorokin, S.P. 1968. Reconstructions of centriole formation and ciliogenesis in mammalian lungs. *J. Cell Sci.* 3:207–230.

Steere, N., V. Chae, M. Burke, F.Q. Li, K. Takemaru, and R. Kuriyama. 2012. A Wnt/beta-catenin pathway antagonist Chibby binds Cenexin at the distal end of mother centrioles and functions in primary cilia formation. *PLoS ONE*. 7:e41077. http://dx.doi.org/10.1371/journal.pone.0041077

Stripp, B.R., S.D. Reynolds, I.M. Boe, J. Lund, J.H. Power, J.T. Coppens, V. Wong, P.R. Reynolds, and C.G. Plopper. 2002. Clara cell secretory protein deficiency alters clara cell secretory apparatus and the protein composition of airway lining fluid. *Am. J. Respir. Cell Mol. Biol.* 27:170–178. http://dx.doi.org/10.1165/ajrcmb.27.2.200200270c

Takemaru, K., S. Yamaguchi, Y.S. Lee, Y. Zhang, R.W. Carthew, and R.T. Moon. 2003. Chibby, a nuclear beta-catenin-associated antagonist of the Wnt/Wingless pathway. *Nature*. 422:905–909. http://dx.doi.org/10.1038/nature01570

Tanos, B.E., H.J. Yang, R. Soni, W.J. Wang, F.P. Macaluso, J.M. Asara, and M.F. Tsou. 2013. Centriole distal appendages promote membrane docking, leading to cilia initiation. *Genes Dev.* 27:163–168. http://dx.doi.org/10.1101/gad.207043.112

Tateishi, K., Y. Yamazaki, T. Nishida, S. Watanabe, K. Kunimoto, H. Ishikawa, and S. Tsukita. 2013. Two appendages homologous between basal bodies and centrioles are formed using distinct *Odf2* domains. *J. Cell Biol.* 203:417–425. http://dx.doi.org/10.1083/jcb.201303071

Vladar, E.K., and T. Stearns. 2007. Molecular characterization of centriole assembly in ciliated epithelial cells. *J. Cell Biol.* 178:31–42. http://dx.doi.org/10.1083/jcb.200703064

Voronina, V.A., K. Takemaru, P. Treuting, D. Love, B.R. Grubb, A.M. Hajjar, A. Adams, F.Q. Li, and R.T. Moon. 2009. Inactivation of Chibby affects function of motile airway cilia. *J. Cell Biol.* 185:225–233. http://dx.doi.org/10.1083/jcb.200809144

Westlake, C.J., L.M. Baye, M.V. Nachury, K.J. Wright, K.E. Ervin, L. Phu, C. Chalouni, J.S. Beck, D.S. Kirkpatrick, D.C. Slusarski, et al. 2011. Primary cilia membrane assembly is initiated by Rab11 and transport protein particle II (TRAPPII) complex-dependent trafficking of Rabin8 to the centrosome. *Proc. Natl. Acad. Sci. USA*. 108:2759–2764. http://dx.doi.org/10.1073/pnas.1018823108

You, Y., E.J. Richer, T. Huang, and S.L. Brody. 2002. Growth and differentiation of mouse tracheal epithelial cells: selection of a proliferative population. *Am. J. Physiol. Lung Cell. Mol. Physiol.* 283:L1315–L1321.